metals

MDPI

Article

Corrosion Behavior of Steels in LiBr–H_2O–$CaCl_2$–$LiNO_3$ Systems

Ana Karen Larios-Galvez [1], Roy Lopez-Sesenes [2], Estela Sarmiento-Bustos [3], Isai Rosales [1], Jorge Uruchurtu-Chavarin [1], Jesus Porcayo-Calderon [4] and Jose Gonzalo Gonzalez-Rodriguez [1,*]

1 Centre for Research in Engineering and Applied Sciences, Autonomous University of the State of Morelos, Cuernavaca 62209, Mexico; karengalvex@gmail.com (A.K.L.-G.); faye12@uaem.mx (I.R.); juch25@uaem.mx (J.U.-C.)
2 Faculty of Chemical Sciences and Engineering, Autonomous University of the State of Morelos, Cuernavaca 62209, Mexico; rlopez@uaem.mx
3 Division of Industrial Mechanics, Emiliano Zapata Technological University of the State of Morelos, Emiliano Zapata 62565, Mexico; estelasarmiento@utez.edu.mx
4 Department of Chemical Engineering and Metallurgy, University of Sonora, Hermosillo 83000, Mexico; jporcayoc@gmail.com
* Correspondence: ggonzalez@uaem.mx

Abstract: Conventional absorption and refrigeration systems use a LiBr/H_2O mixture, which causes corrosion problems to the metallic components. In order to avoid this and some other problems such as crystallization and vapor pressure, some additives such as $CaCl_2$ and/or $LiNO_3$ are added to the LiBr/H_2O mixture. In the present work, the corrosion behavior of 1018 carbon steel as well as of type 304 and 316L stainless steels was evaluated in LiBr/H_2O at 80 °C with the addition of $CaCl_2$, $LiNO_3$, and $CaCl_2$+$LiNO_3$. Potentiodynamic polarization curves and electrochemical impedance spectroscopy were used for this purpose. The results showed that the corrosion current density values of all tested steels decreased with the addition of $CaCl_2$ and/or $LiNO_3$, which induced the formation of a passive film on carbon steel. Both types of stainless steels showed a passive film in all tested conditions, but the passive current density was the lowest, whereas the passive zone was the widest, for 316L steel. The corrosion mechanism remained unaltered for both stainless steels but was changed with the addition of $CaCl_2$ and/or $LiNO_3$ for carbon steel.

Keywords: LiBr; carbon steel; stainless steels; pitting corrosion

check for updates

Citation: Larios-Galvez, A.K.; Lopez-Sesenes, R.; Sarmiento-Bustos, E.; Rosales, I.; Uruchurtu-Chavarin, J.; Porcayo-Calderon, J.; Gonzalez-Rodriguez, J.G. Corrosion Behavior of Steels in LiBr–H_2O–$CaCl_2$–$LiNO_3$ Systems. *Metals* **2022**, *12*, 279. https://doi.org/10.3390/met12020279

Academic Editor: Santiago Fajardo

Received: 17 December 2021
Accepted: 28 January 2022
Published: 3 February 2022

Publisher's Note: MDPI stays neutral with regard to jurisdictional claims in published maps and institutional affiliations.

Copyright: © 2022 by the authors. Licensee MDPI, Basel, Switzerland. This article is an open access article distributed under the terms and conditions of the Creative Commons Attribution (CC BY) license (https://creativecommons.org/licenses/by/4.0/).

1. Introduction

Absorption refrigeration systems are compression refrigeration systems that use thermal compressors [1–3]. Such systems have the advantages of reduced electricity consumption and low maintenance costs. The absorption refrigeration system is a heat-operated unit that uses a refrigerant that is alternately absorbed by and liberated from the absorbent [4]. Two working fluids are employed in the system, a refrigerant and an absorbent. In commercial manufacturing products, the most widely solution pair which is commonly used is lithium bromide/water (LiBr/H_2O) [5–8] due to its excellent thermophysical properties, although it can cause serious corrosion problems to the metallic components of the system, as widely documented [9–15]. In order to decrease the corrosion problems as well as those associated with solubility, crystallization temperature, vapor pressure, chemical and thermal stability, among others, many research works have been carried out. Thus, Li [16] used the ternary mixture $CaCl_2$–LiBr–$LiNO_3$ for an absorption system based on one step that uses solar energy, whereas Li [17] carried out a study by using the $CaCl_2$–$LiNO_3$–KNO_3/H_2O quaternary system. Both studies showed a decrease in the vapor pressure and in the crystallization temperature. Torres [18] analyzed the efficiency of an absorption thermal transformer by using as an absorber the quaternary mixture LiBr–LiI–$LiNO_3$–LiCl/H_2O, where the addition of Li salts improved LiBr solubility. Although LiBr possesses excellent thermophysical properties, which make it one of the most widely used compounds in

cooling systems, it can cause significant corrosion problems to the materials used in these systems such as carbon steel and stainless steels [19–29]. Due to its low cost, carbon steel was widely used in these systems, but it suffers from severe corrosion problems in a LiBr solution. Austenitic stainless steels have been used instead of carbon steel due to their higher corrosion resistance in a halide-containing environment. However, it was found that stainless steels were very susceptible to the pitting type of corrosion, causing failures in these systems. Another halide that induces high corrosion rates in stainless steels is calcium chloride, $CaCl_2$, although, as time elapses, a passive layer is formed with a decrease in the corrosion rate [30,31]. One of the most widely used methods to prevent corrosion problems is the use of corrosion inhibitors, including anodic ones such as chromates, molybdates, and nitrates [14–24], due to the formation of a passive layer which protects metals against corrosion. Thus, on one hand, halides such as Br and Cl promote high corrosion rates, while, on the other hand, protective passive layers induced by $CaCl_2$ and $LiNO_3$ are formed. The combined effect of LiBr, $CaCl_2$, and $LiNO_3$ on the corrosion behavior of materials used in cooling systems is not known. Although many non-ferrous alloys such as Cu–Ni, Titanium-, Nickel- and Copper-base alloys have been studied with respect to their corrosion behavior in a LiBr/H_2O system [19–29], many research works have been undertaken on ferrous alloys such as carbon steel and stainless steels [12–15,32,33]. Carbon steel is widely used as a structural metallic component in absorption cooling systems due to its low cost, although it suffers from severe corrosion problems, which makes it necessary to evaluate some other more corrosion-resistant ferrous alloys such as austenitic type 304 and 316L stainless steels, although they are susceptible to localized corrosion. Thus, the aim of the present work was to evaluate the corrosion resistance of 1018 carbon steel as well as of type 304 and 316L stainless steels in a LiBr/H_2O mixture with the addition of $CaCl_2$ and/or $LiNO_3$.

2. Experimental Procedure

2.1. Testing Materials

The ferrous testing materials used in this research work included, as mentioned above, 1018 carbon steel and type 304 and 316L austenitic stainless steels, whose chemical composition is shown in Table 1. For this purpose, commercial cylindrical bars, 6 mm in diameter, were obtained. Specimens measuring 10 mm in length were cut and encapsulated in a commercial polymeric resin. They were abraded with 600–4000-grade emery paper, washed, and cleaned with acetone.

Table 1. Chemical composition of the steels used in the present research work (wt.%).

Steel	Cr	Ni	Mo	Mn	C	P	S	Fe
1018	-	-	-	0.90	0.14	0.03	0.03	balance
304	18.5	7.8	0.14	1.4	0.05	0.04	0.03	balance
316L	16.7	10.8	2.3	1.6	0.02	0.04	0.03	balance

2.2. Testing Solution

Tests were carried out using LiBr/H_2O as a base solution at the concentration of 850 g/L [33]. Calcium chloride ($CaCl_2$) and lithium nitrate ($LiNO_3$) were added separately and in combination, i.e., $CaCl_2$–LiBr (1.35:1)/H_2O [16], LiBr–$LiNO_3$ (4:1)/H_2O [34], and $CaCl_2$–LiBr–$LiNO_3$ (8.72:1:1)/H_2O [35]. Most of the reported research works used working temperatures between 30 and 150 °C [19–29]. Since electrochemical cells to carry out tests at temperatures higher than 80 °C were not available, this was chosen as the working temperature.

2.3. Electrochemical Techniques

Potentiodynamic polarization curves and electrochemical impedance spectroscopy (EIS) techniques were used. For this, a standard electrochemical glass cell with three

electrodes was used. A silver/silver chloride (Ag/AgCl) electrode was used as the reference electrode, whereas a 6 mm-diameter graphite rod was used as the auxiliary electrode. Before starting the tests, the open circuit potential value (OCP) was allowed to stabilize and was monitored during one hour. Once the OCP value was stable, scanning started for the polarization curves, starting at a potential value 600 mV more negative than the free corrosion potential, E_{corr}, and scanned into the anodic direction at a sweep rate of 0.1667 mV/s, ending at a potential value 600 mV more anodic than E_{corr}. Corrosion current density values, I_{corr}, were calculated with the aid of the Tafel extrapolation method. Finally, EIS experiments were carried out at the E_{corr} and by applying a sinusoidal peak-to-peak signal of 10 mV at frequency intervals of 0.1–100 kHz, with the aid of a potentiostat from ACM Instruments. Selected corroded specimens were analyzed in a low vacuum LEO 1450VP scanning electronic microscope. A schematic diagram of the experimental set-up is shown in Figure 1.

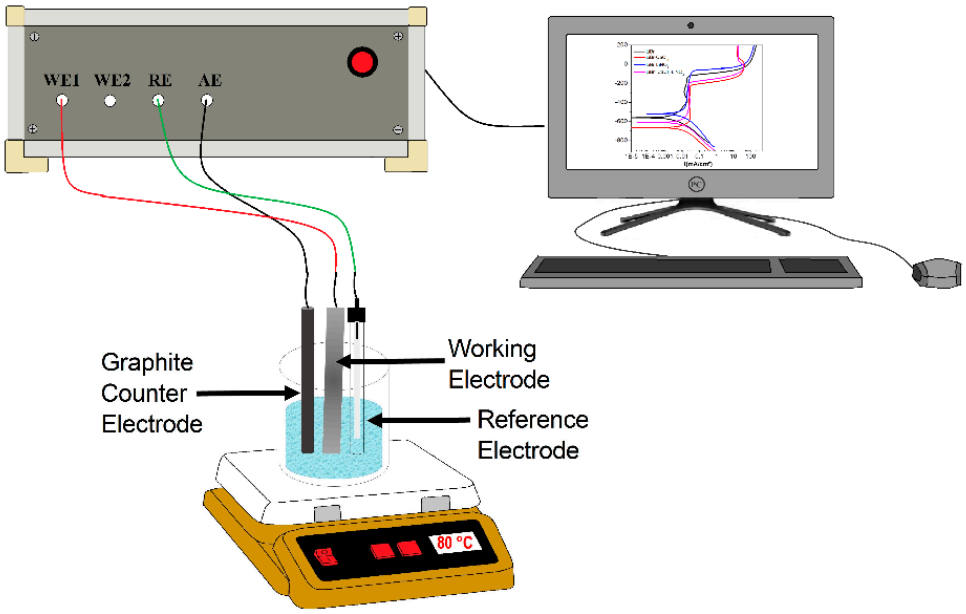


Figure 1. Schematic diagram showing the experimental set-up.

3. Results and Discussion

3.1. Open Circuit Potential Values

The variation of the OCP value with time for 1018 carbon steel as well as for type 304 and 316L stainless steels in the LiBr/H_2O mixture with the addition of $CaCl_2$ and/or $LiNO_3$ at 80 °C can be seen in Figure 2. This figure shows that the addition of $CaCl_2$ to LiBr/H_2O caused a shift of the OCP value for 1018 carbon steel towards more active values as compared to the value obtained in LiBr/H_2O, as shown in Figure 2a, since for the latter, the OCP value was close to −550 mV, whereas for the former, it was between −640 and −610 mV. Most reported results show that carbon and stainless steels exhibit high corrosion rates when exposed to $CaCl_2$ solutions. For instance, in [29,30], it is reported that an increase in the testing temperature from 30 to 80 °C brought an increase in the corrosion current density value during the first hours of testing, but after that time, a layer of corrosion products formed on top of the steel, determining a decrease in the corrosion current density value. Similar results were reported in [31] for the working pair consisting of LiBr/H_2O+$CaCl_2$. On the other hand, the addition of $LiNO_3$ shifted the OCP value into the noble direction, whereas that of $CaCl_2$+$LiNO_3$ shifted it towards more active values, which as reported in a high number of research works, lead to the formation of passive layers on top of carbon and stainless steels [36–39].

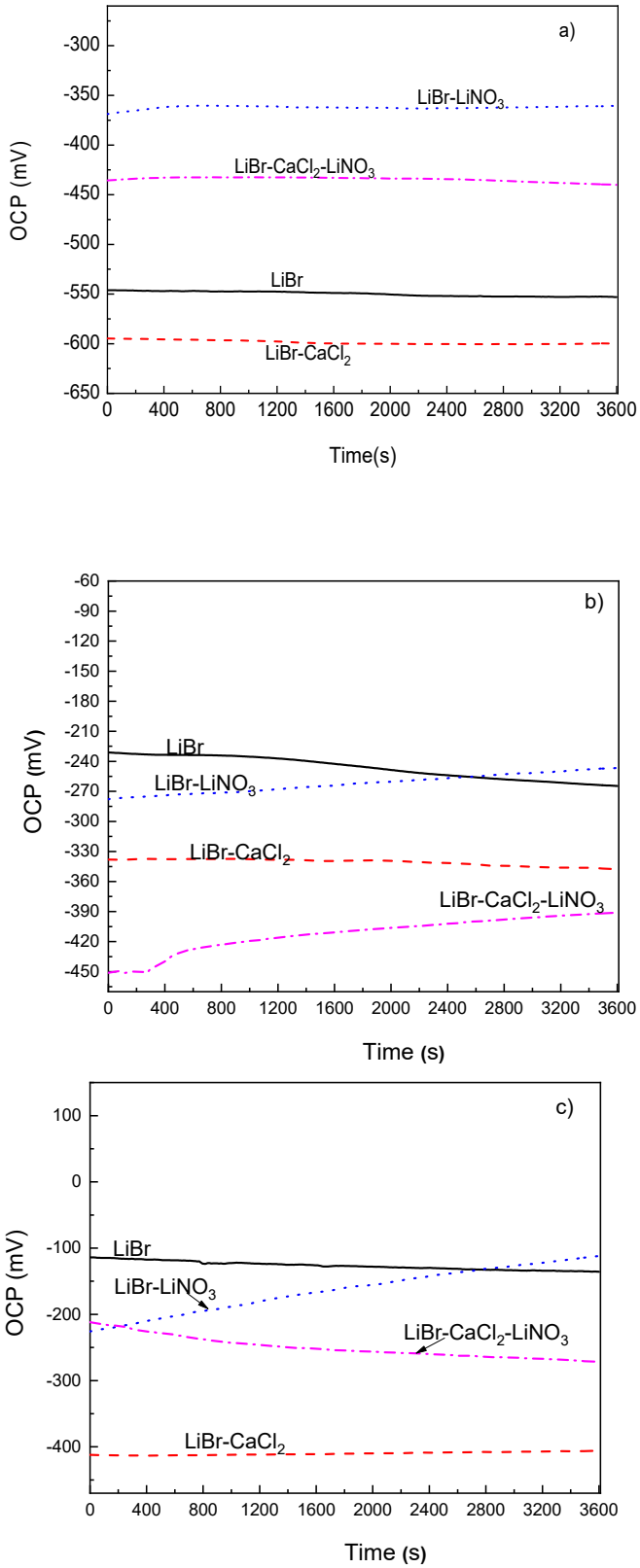


Figure 2. Variation of the OCP value for (**a**) 1018 carbon steel, (**b**) type 304 and (**c**) 316L stainless steels in LiBr/H_2O with the addition of $CaCl_2$ and $LiNO_3$.

For type 304 and 316L stainless steels (Figure 2b,c), the OCP values were, generally speaking, nobler than those obtained for 1018 carbon steel. Thus, the OCP value in the LiBr/H_2O mixture was close to −550 mV for 1018 carbon steel; for 304 stainless steel, it

started at a value close to −235 mV and finished at a potential value of −265 mV, while for 316L steel, it started at a value of −110 mV and finished at a potential value of −135 mV. According to this, the lowest susceptibility towards corrosion in this environment was observed for 316L steel. Similarly, for both stainless steels, the addition of $CaCl_2$ and/or $LiNO_3$ to the $LiBr/H_2O$ mixture made the OCP value to shift towards more active values. One exception was observed with the addition of $LiNO_3$, which at the beginning of the test, shifted the OCP values towards slightly more active values, but after 2400 s of exposure, caused the OCP value to become either equal to or slightly nobler than those obtained in the $LiBr/H_2O$ mixture. One very important feature to note is that for the three steels, the OCP values remained very constant as time elapsed, regardless of the addition of $CaCl_2$ and/or $LiNO_3$, even in the $LiBr/H_2O$ mixture, which indicated the stability of the corrosion products layer on top of the steels.

3.2. Potentiodynamic Polarization Curves

Thermodynamic parameters such as the OCP value only provide the trend of a metal towards corrosion but do not say anything about corrosion kinetics. Polarization curves not only provide parameters such as the corrosion current density value, I_{corr}, but also provide information on the processes taking place on a metal surface, such as passivation, pitting corrosion, oxygen reduction, and hydrogen evolution reactions, among others. Polarization curves for 1018 carbon steel and type 304 and 316L stainless steels in the $LiBr/H_2O$ solution containing $CaCl_2$ and $LiNO_3$ are shown in Figure 3.

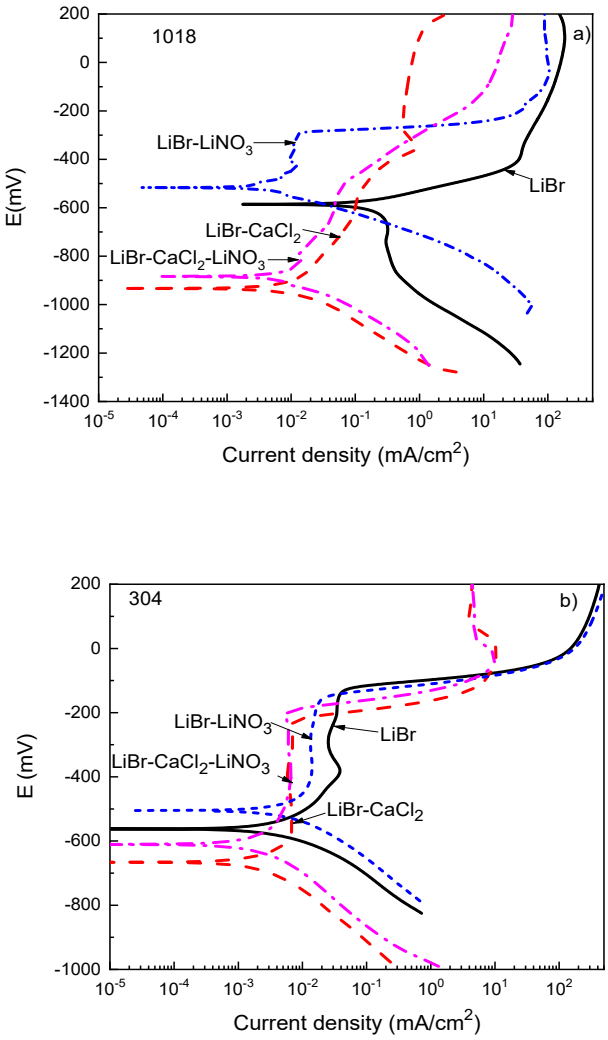


Figure 3. *Cont.*

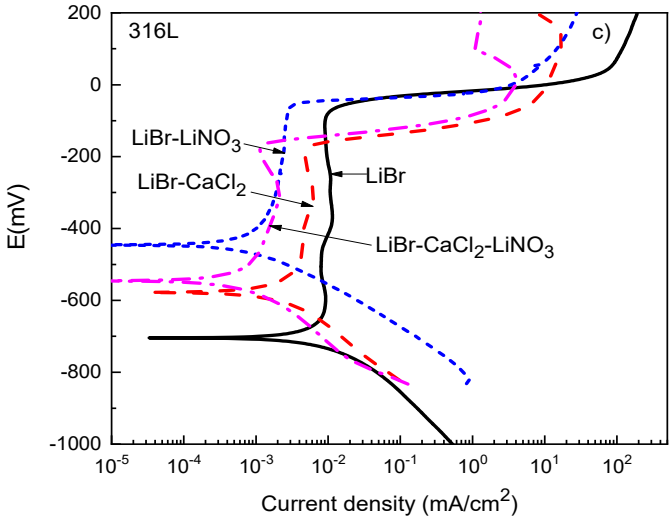


Figure 3. Effect of the addition of $CaCl_2$ and $LiNO_3$ to $LiBr/H_2O$ on the OCP values for (**a**) 1018 carbon steel, (**b**) type 304, and (**c**) type 316L stainless steels.

For 1018 carbon steel in the $LiBr/H_2O$ solution (Figure 3a), the polarization curve showed only an active behavior, and there was no evidence of the formation of a passive film on the anodic branch of the curve, with a very rapid increment on the anodic current density at low anodic overpotentials; after that, the anodic current density increased in a slower way due to the formation of a corrosion products layer, which, according to Tanno et al. [39], consists basically of magnetite, Fe_3O_4, although Guo et al. [38] reported the presence of Fe_2O_3 which can be explained according to following reactions:

Anodic reaction:

$$3Fe \rightarrow 3Fe^{2+} + 6e \quad (1)$$

$$2Fe + 60H^{-} \rightarrow Fe_2O_3 + 3H_2O + 6e \quad (2)$$

Cathodic reaction:

$$2H_2O + 2e \rightarrow 2OH^{-} + H_2 \quad (3)$$

whereas the formation of Fe_3O_4 can be explained according to:

$$Fe^{2+} + H_2O \rightarrow FeOH^{+} + H^{+} \quad (4)$$

$$3FeOH^{+} + H_2O \rightarrow Fe_3O_4 + 5H^{+} + 2e \quad (5)$$

$$2H^{+} + e \rightarrow H_2 \quad (6)$$

On the cathodic branch, on the other hand, a cathodic limit current density due to the oxygen reduction reaction was observed from the E_{corr} value down to a potential value of −900 mV; for potentials more cathodic than 900 mV, the hydrogen evolution reaction was present. When $CaCl_2$, $LiNO_3$, or their combination was added to the $LiBr/H_2O$ solution, the presence of a passive layer was evident on the anodic branch of the polarization curves, as well as a decrease in the I_{corr} value. Similar results were found by Sarmiento-Bustos [40] for 1018 carbon steel in an $LiBr/H_2O$ + ethylene glycol mixture with the addition of $LiNO_3$. The polarization curve in absence of $LiNO_3$ did not show the presence of a passive layer, but in the presence of $LiNO_3$, a passive zone was evident, attributed to the addition of $LiNO_3$ which is well known to act as an anodic, passivating inhibitor [38–42]; in addition, it has been established that nitrates are incorporated into the film [43]. As established above, most of the reported results show that carbon and stainless steels exhibit high corrosion rates when exposed to $CaCl_2$ solutions but, after some time, this corrosion rate slows down due to the formation of a passive layer consisting of iron oxide in the case of carbon steel [38,39]. The passive film in the presence of $LiNO_3$ was very stable, more or less 100 mV wide, with

the passive current density remaining very stable with the applied potential. The passive current density values in the presence of either $CaCl_2$ or $CaCl_2$+$LiNO_3$ did not remain constant with the applied constant, but increased in a slow fashion.

For type 304 and 316L stainless steels (Figure 3b,c), the polarization curves in the LiBr/H_2O mixture exhibited a passive zone which was wider for the latter, since for 304 steel, it started at a potential value close to −400 mV and ended at a pitting potential value around −150 mV, i.e., it was 250 mV wide, whereas for 316L steel, it started at a potential value of −650 mV and ended at a pitting potential value of −50 mV, i.e., it was 700 mV wide. It has been very well documented that bromide can induce pitting corrosion on stainless steels due to its ability to breakdown passive films [44,45]. In addition to this, the corrosion and passive current density values were higher for type 304 than for type 316L stainless steels. The passive film formed on type 304 stainless steel had a dual structure, with an inner chromium oxide/hydroxide layer and an outer layer of iron oxide/hydroxide [45]. The higher Mo amount contained in type 316L stainless steel led to the formation of a more stable passive film on the latter because of the incorporation of molybdenum oxide into the chromium oxide film [43,44]. It was established above that the pitting potential for 304 steel was −150 mV, whereas that for 316L stainless steel was −50 mV. Both the corrosion and the passive current density values were lowered with the addition of $CaCl_2$ and/or $LiNO_3$. The lowest passive current density for type 304 steel was obtained when either $CaCl_2$ alone or in combination with $LiNO_3$ was added, whereas for 316L steel, this value was obtained with the addition of $LiNO_3$ either alone or in combination with $CaCl_2$. In both steels, a reduction of the passive current density value by nearly one order of magnitude was obtained.

A summary of the variation of the I_{corr} value for the three steels in the LiBr/H_2O mixture in the absence and presence of $CaCl_2$ and/or $LiNO_3$ is shown in Figure 4. This figure shows that the highest I_{corr} values were obtained for 1018 carbon steel, whereas the lowest values were achieved for type 316L stainless steels. The addition of $CaCl_2$ and/or $LiNO_3$ to the LiBr/H_2O mixture decreased the I_{corr} values regardless of the steel by at least one order of magnitude. For 1018 carbon steel, the lowest I_{corr} value was obtained when $CaCl_2$ was added to the system, whereas for both type 304 and 316L stainless steels, the lowest I_{corr} value was obtained with the addition of the mixture of $CaCl_2$+$LiNO_3$.

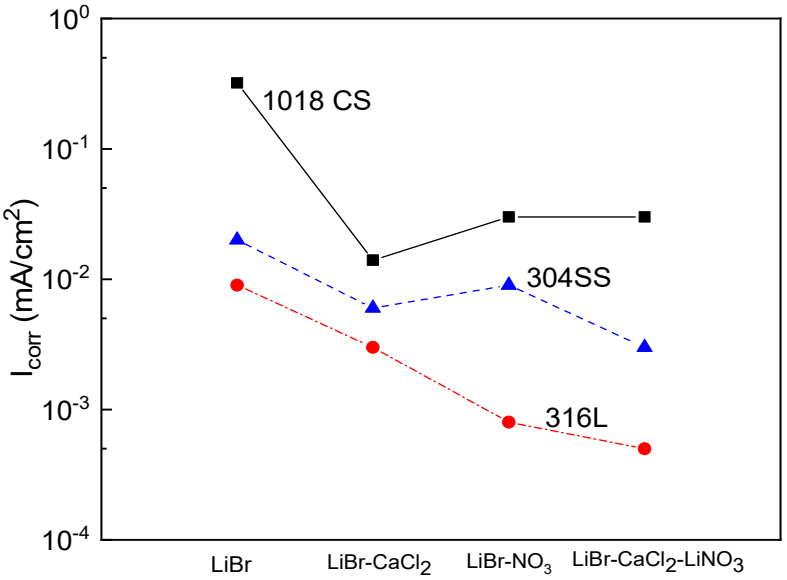


Figure 4. Effect of the addition of $CaCl_2$ and $LiNO_3$ to LiBr/H_2O on the I_{corr} values for 1018 carbon steel and type 304 and 316L stainless steels.

3.3. Electrochemical Impedance Spectroscopy

EIS data provide information on the involved corrosion mechanism. Nyquist diagrams for different steels in the LiBr/H_2O mixture with the addition of $CaCl_2$ and $LiNO_3$ are presented in Figure 5, whereas the corresponding Bode plots are shown in Figure 6.

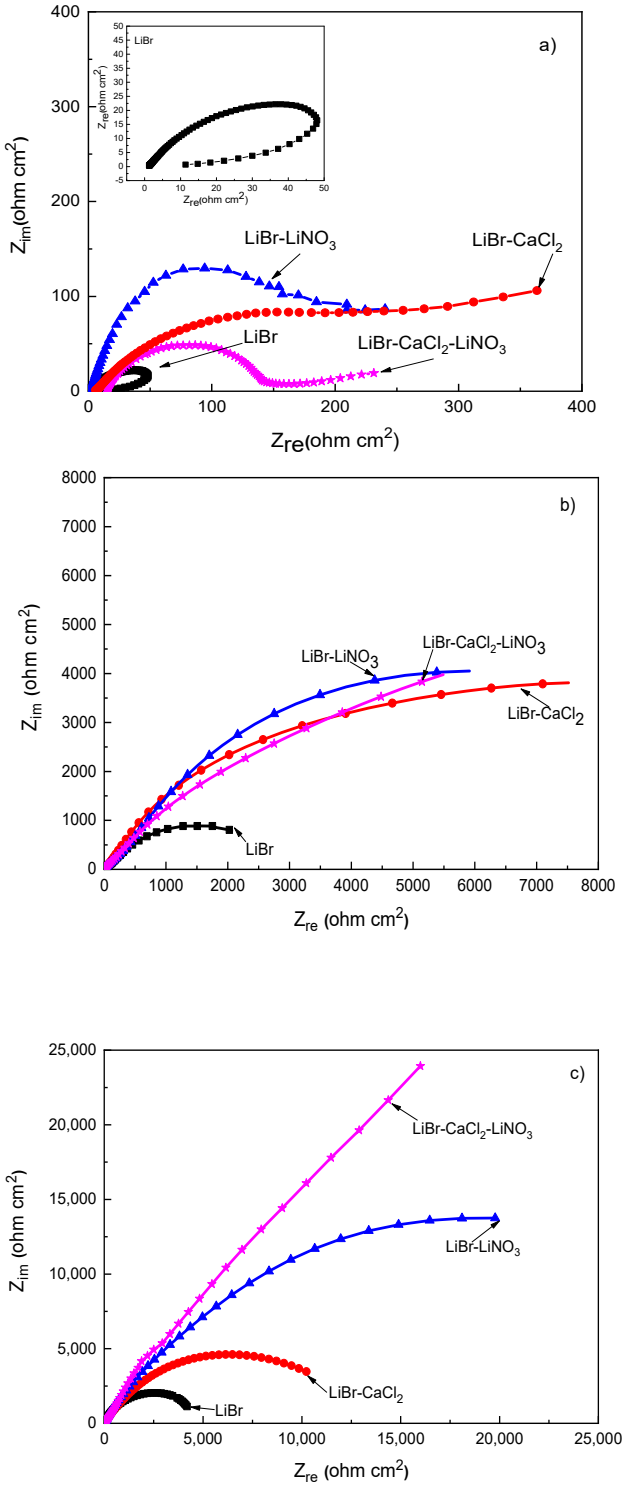


Figure 5. Effect of the addition of $CaCl_2$ and $LiNO_3$ to LiBr/H_2O on the Nyquist plots for (**a**) 1018 carbon steel, (**b**) type 304, and (**c**) type 316L stainless steels.

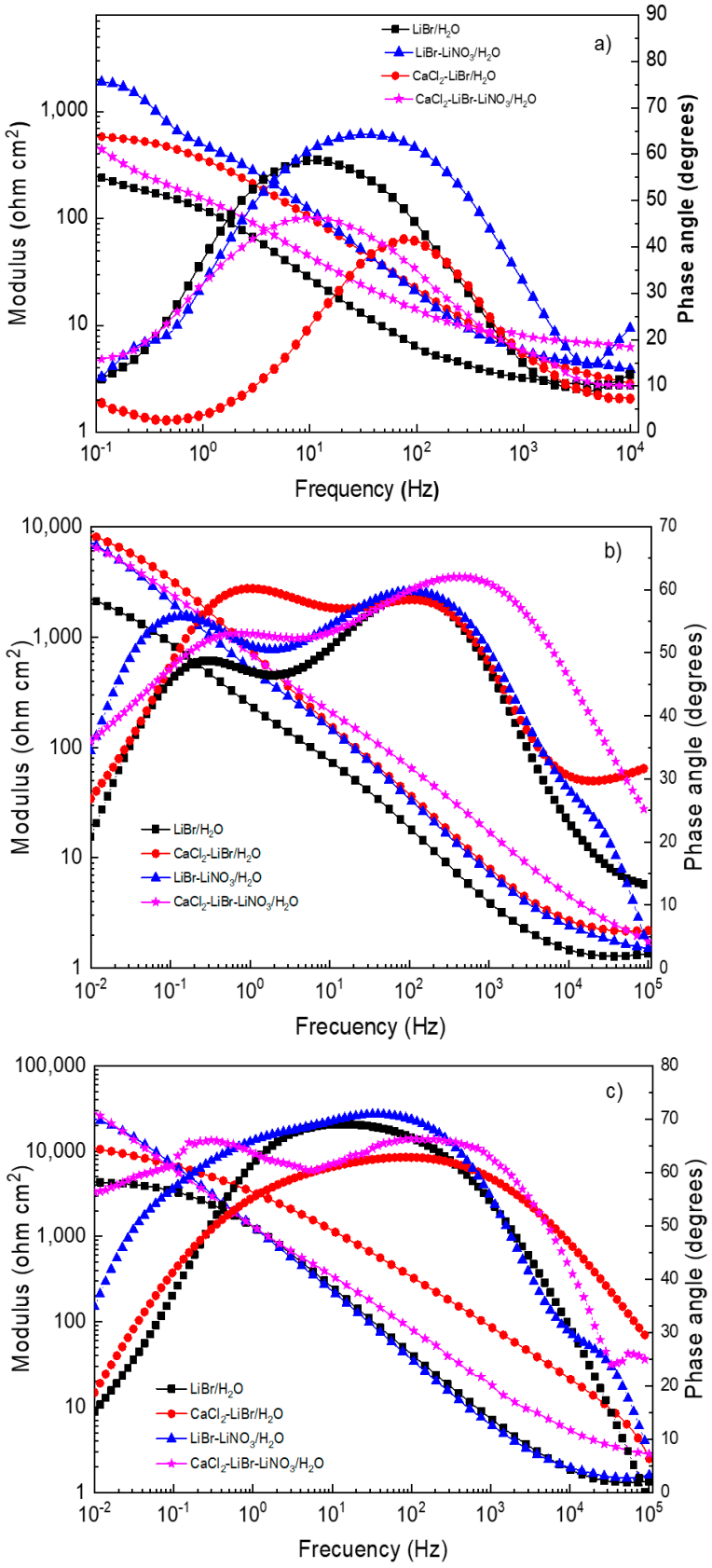


Figure 6. Effect of the addition of $CaCl_2$ and $LiNO_3$ to $LiBr/H_2O$ on Bode plots for (**a**) 1018 carbon steel, (**b**) type 304, and (**c**) 316L stainless steels.

The Nyquist diagram for 1018 carbon steel, Figure 5a, shows the presence of a depressed, capacitive semicircle at high and medium values of frequency, whereas at the lowest frequencies, an inductive loop is present in the LiBr/H_2O system only, probably due to the adsorption/desorption of some intermediate species such as $FeOH^+$ in Equation (4), whose adsorption and desorption control the corrosion reaction. The semicircle shape changed, and thus, the corrosion mechanism, with the addition of either $CaCl_2$ and/or $LiNO_3$ to the LiBr/H_2O system, since the inductive semicircle disappeared, and, in addition to the observed capacitive loop at high and intermediate values of frequency, a second capacitive loop was observed at the lowest frequency values for 1018 carbon steel; in contrast, for both stainless steels, a single capacitive loop was observed at all frequency values. The semicircle observed at high and intermediate frequency values was attributed to the electrochemical reactions taking place at the metal/double electrochemical layer interface, whereas the lowest frequency semicircle was related to the electrochemical reactions taking place at the metal/corrosion products film interface. The high frequency semicircle diameter was the smallest in the LiBr/H_2O mixture, whereas it increased when $CaCl_2$ and/or $LiNO_3$ were added, reaching the highest value when $CaCl_2$ was added.

On the other hand, for both type 304 and 316L stainless steels, Figure 5b,c, the Nyquist diagrams displayed a single depressed, capacitive semicircle at all frequency values, indicating a charge transfer-controlled corrosion process. In both cases, the smallest semicircle diameter was observed in the LiBr/H_2O mixture and increased considerably with the addition of $CaCl_2$ and/or $LiNO_3$. The real impedance values obtained for the 316L type stainless steel were higher than those obtained for 304 steel at all tested conditions, which, in turn, where higher than those obtained for 1018 carbon steel. This increase in the semicircle diameter for 304 type stainless steel as compared to that obtained for 1018 carbon steel in the LiBr/H_2O mixture was due to the presence of a compact, highly protective chromium oxide/hydroxide layer [45] whereas the presence of more Mo in 316L steel led to the formation of a more stable passive film on the latter because of the incorporation of molybdenum oxide into the chromium oxide film [44]. As mentioned above, for 1018 carbon steel, the corrosion products film consisted mainly of Fe_3O_4, with some Fe_2O_3 [41], which are not protective as a chromium oxide layer. When exposed to $CaCl_2$ solutions, the corrosion rate of carbon and stainless steels was high but, after some time, it slowed down due to the formation of a passive layer consisting of iron oxide in the case of carbon steel [38,39]. This led to an increase in the real impedance values for the three tested steels. Finally, the addition of $LiNO_3$ formed a passive film, since it is well known to act as an anodic, passivating inhibitor [38,39]. It has been established that nitrates are incorporated into the film [43,44], which is the reason of the observed semicircle diameter when $LiNO_3$ was added to the LiBr/H_2O mixture.

The Bode diagrams for 1018 carbon steel, Figure 6a, show that the lowest absolute impedance values at the maximum frequency were obtained in the LiBr/H_2O mixture and increased with the addition of $CaCl_2$ and/or $LiNO_3$, leading to the highest value when $LiNO_3$ was introduced due to the formation of passive layers, as explained above. On the other hand, phase angle data revealed a single peak when 1018 carbon steel was exposed to the LiBr/H_2O mixture, suggesting that the formation of a protective layer on top of the steel did not occur; however, when $CaCl_2$ and/or $LiNO_3$ were added, the phase angle value increased from 40 up to 70° and remained more or less constant over a wide frequency interval, evidencing of the presence of a passive layer on top of the steel and of two time constants. For both stainless steels (Figure 6b,c) the lowest absolute impedance values at the highest frequency were obtained in the LiBr/H_2O mixture and increased with the addition of $CaCl_2$ and/or $LiNO_3$ in a similar way as that observed for 1018 carbon steel; however, the values for both stainless steels were higher than those for carbon steel. The phase angle values obtained for both stainless steels in the LiBr/H_2O mixture were very close to those obtained with the addition of $CaCl_2$ and/or $LiNO_3$, remaining very constant over a wide frequency interval for 316L type stainless steel, indicative of a very stable, protective

passive layer. For 304 type stainless steel, the phase angle values showed the presence of two peaks, indicating two time constants.3.4. Surface Analysis of Corroded Samples.

Surface samples of 1018 carbon steel corroded in LiBr/H_2O containing $CaCl_2$ and/or $LiNO_3$ are shown in Figure 6. For specimens corroded in the LiBr/H_2O system (Figure 7a), the aggressiveness of the solution produced a very rough steel surface, showing some uniform type of corrosion in combination with an apparently localized, shallow corrosion, similar to pits. The polarization curve in this condition did not show the presence of a passive film; therefore, no pitting type of corrosion was expected. On the other hand, specimens corroded in the presence of $CaCl_2$ (Figure 7b) showed a very smooth surface, indicating that the damage produced by the environment was very low, in combination with some pits. Specimens corroded in LiBr/H_2O+$LiNO_3$ (Figure 7c), showed a smooth surface in combination with a type of localized corrosion, since in this condition, the polarization curve showed evidence of a very stable passive film, very similar to that exhibited by the specimens corroded in the presence of $CaCl_2$ (Figure 7b), where the pitting type of corrosion was expected. Finally, the surface morphology of specimens corroded in LiBr/H_2O+$CaCl_2$+$LiNO_3$ (Figure 7d) exhibited a combination of localized and uniform corrosion, which, according to the polarization curve (Figure 3a), indicated a not very stable passive film, because the passive current density did not remain constant with the applied potential. On the other hand, 304 type stainless steel corroded in LiBr/H_2O (Figure 8a), showed the presence of pits, some of which with a diameter larger than 10 µm, whereas there was no evidence of a general type of uniform corrosion, since the steel surface looked very smooth, a signal that the steel was not corroded by the electrolyte. The polarization curve under all conditions tested showed the presence of a passive layer, and, thus, a great susceptibility towards the pitting type of corrosion, as shown in Figure 3a. When the steel was corroded in LiBr/H_2O+$CaCl_2$ (Figure 8b), the number and size of the pits decreased, and the surface looked rougher, evidence that the addition of $CaCl_2$ increased the solution aggressiveness. On the other side, for the test in LiBr/H_2O+$LiNO_3$ (Figure 8c), the number of pits and their size increased considerably, indicating a greater susceptibility towards the pitting type of corrosion, whereas for the steel corroded in LiBr/H_2O+$CaCl_2$+$LiNO_3$ (Figure 8d), the number of pits present on the metal surface was high but smaller than that found in the test carried out in LiBr/H_2O+$LiNO_3$. The steel surface showed a high roughness due to the solution aggressiveness.

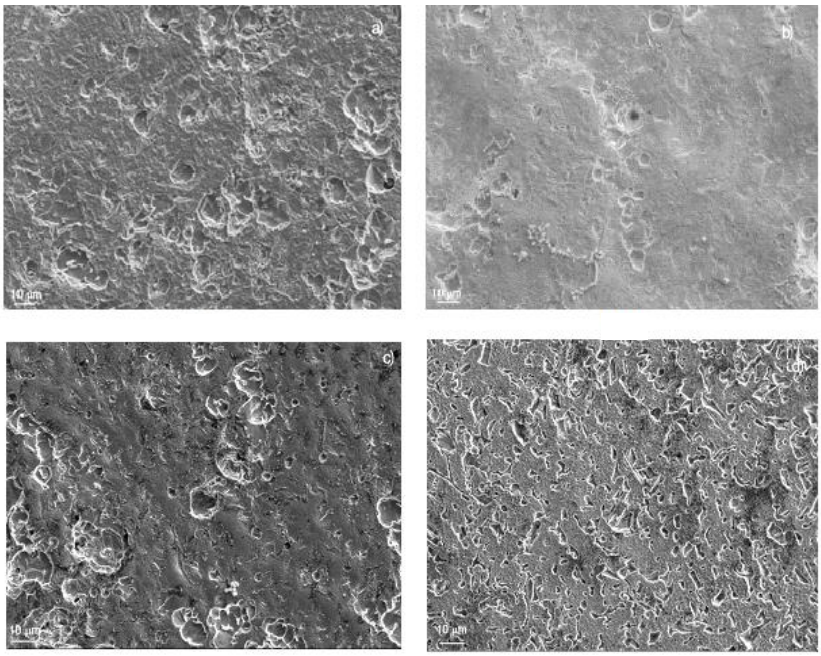


Figure 7. SEM micrograph of 1018 carbon steel corroded in (**a**) LiBr/H_2O, (**b**) LiBr/H_2O+$CaCl_2$, (**c**) LiBr/H_2O+$LiNO_3$, and (**d**) LiBr/H_2O+$CaCl_2$+$LiNO_3$ at 80 °C.

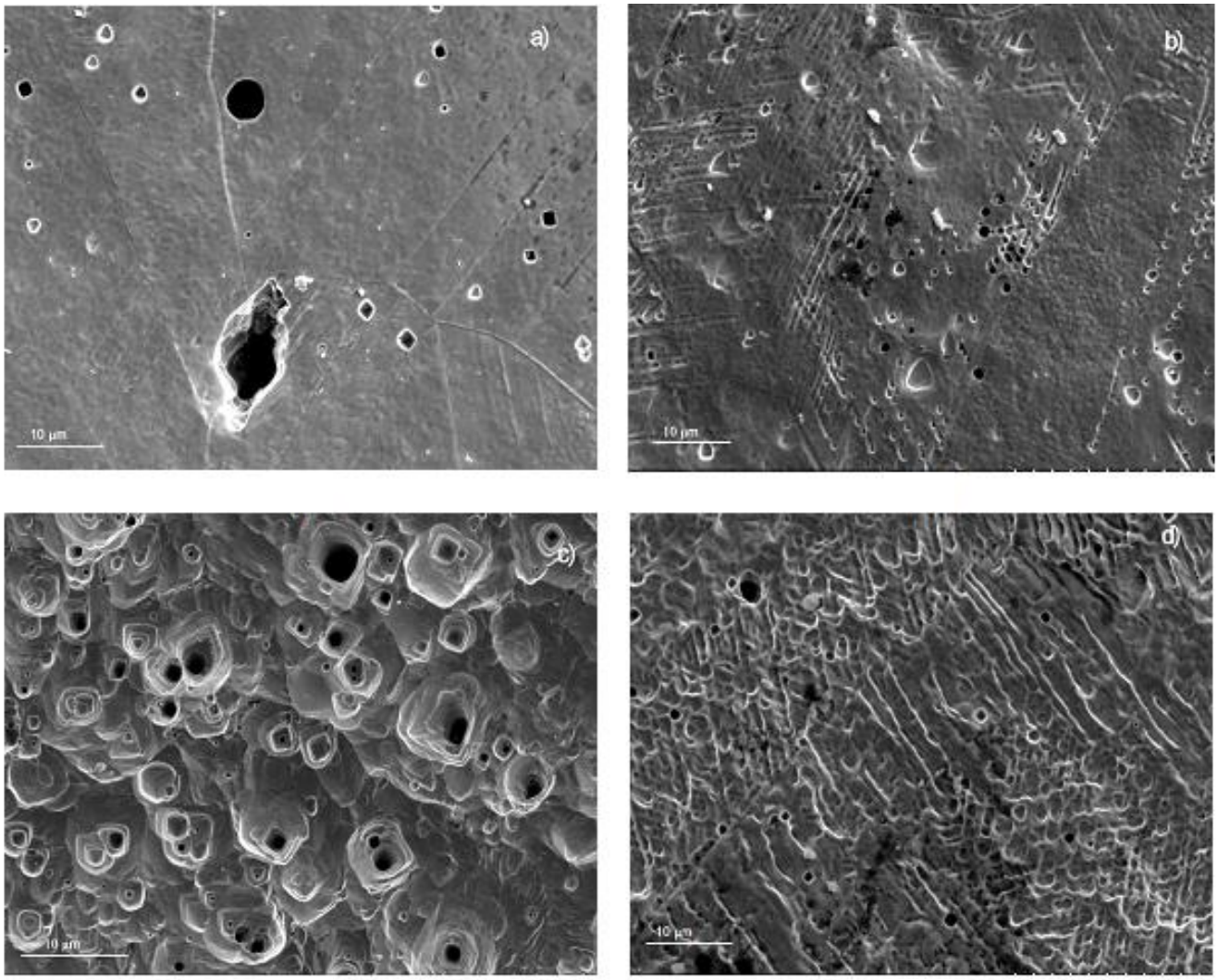


Figure 8. SEM micrograph of 304 stainless steel corroded in (**a**) LiBr/H_2O, (**b**) LiBr/H_2O+$CaCl_2$, (**c**) LiBr/H_2O+$LiNO_3$, and (**d**) LiBr/H_2O+$CaCl_2$+$LiNO_3$ at 80 °C.

According to Figures 3 and 4, 316L type stainless steel exhibited both the lowest I_{corr} values and the widest passive zones, and this was reflected on the damage found on the steels surface in each tested solution, as shown in Figure 9. Unlike the surface morphology displayed by 304 steel in the LiBr/H_2O solution, exhibiting a relatively high number of pits, some of them with a diameter larger than 10 µm, the surface of 316L steel corroded in this solution showed the presence of a few pits, with a diameter smaller than 1.0 µm, together with some seemingly shallow pits, with diameters between 5 and 10 µm, and a very smooth surface, indicative of the absence of a uniform type of corrosion, as shown in Figure 9a. On the other hand, the surface morphology of steel tested in LiBr/H_2O+$CaCl_2$ (Figure 9b), exhibited the presence of a similar number of pits, also similar in size, as that found for steel tested in LiBr/H_2O. However, the steel surface looked rougher, indicating a greater damage due to the action of the electrolyte. For specimens corroded in LiBr/H_2O+$LiNO_3$ (Figure 9c), a smooth surface with a few, shallow pits was observed, indicating that the steel did not suffer from a uniform type of corrosion, but only underwent localized corrosion. The pit size was smaller than that observed for steel tested in LiBr/H_2O. Finally, for specimens tested in LiBr/H_2O+$CaCl_2$+$LiNO_3$ (Figure 9d), a rough surface was observed, evidence of the damage caused by the solution to the steel; however, the surface did not show evidence of a very high damage. A summary of the different observed morphologies is provided in Table 2.

Table 2. Observed morphology of the corroded surfaces for the different tested steels in $LiBr/H_2O$ with $CaCl_2$ and/or $LiNO_3$.

Steel/ Environment	$LiBr/H_2O$	$LiBr/H_2O+CaCl_2$	$LiBr/H_2O+LiNO_3$	$LiBr/H_2O+CaCl_2$ $LiNO_3$
1018	Uniform corrosion + shallow pits	Uniform corrosion + few pits	Uniform corrosion + few pits	High number of pits
304	Pits	Less, shallower pits	More, bigger pits	More, smaller pits
316L	Pits	Much Less, smaller pits	Less, smaller pits	No pits

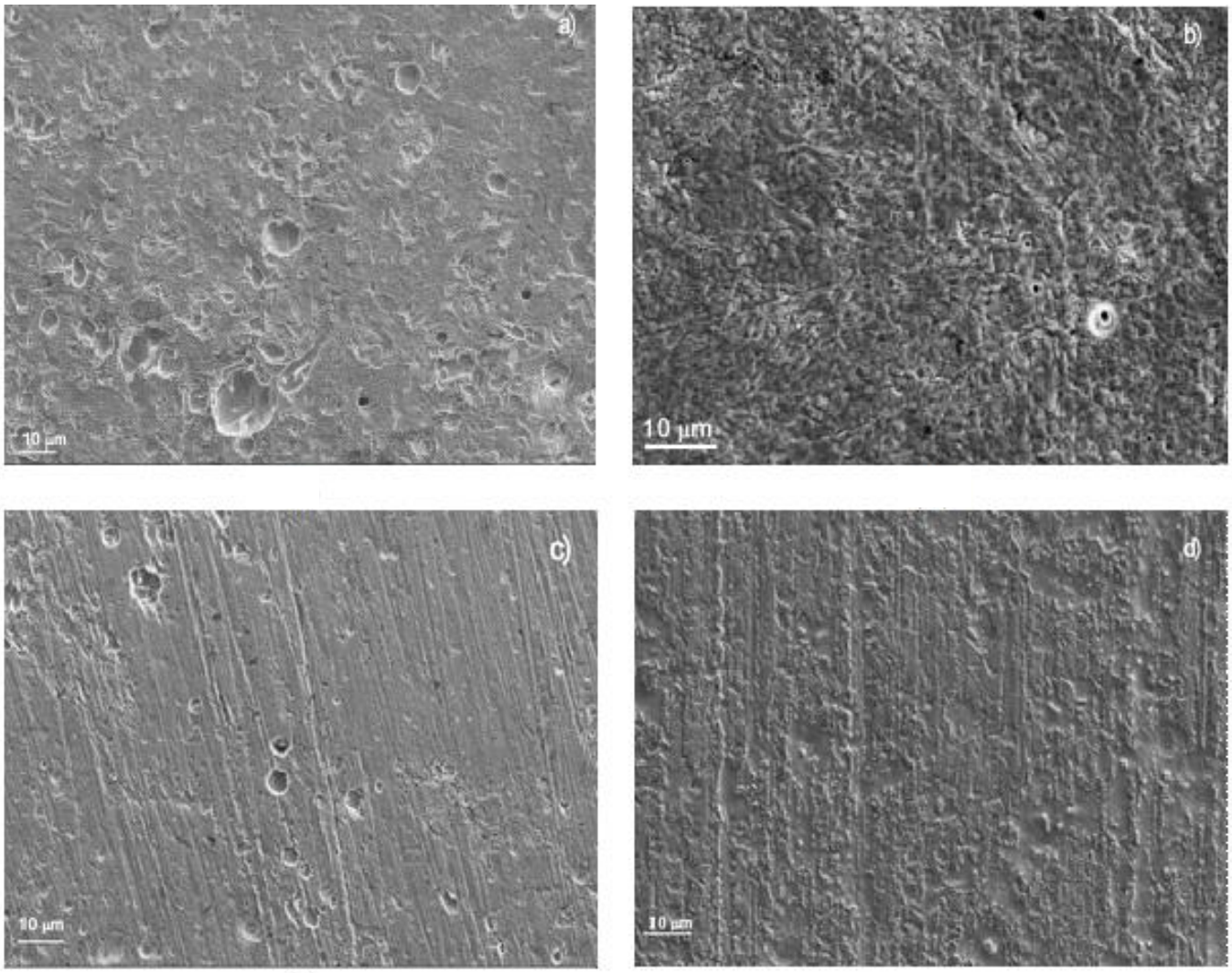


Figure 9. SEM micrograph of 316L stainless steel corroded in (**a**) $LiBr/H_2O$, (**b**) $LiBr/H_2O+CaCl_2$, (**c**) $LiBr/H_2O+LiNO_3$, and (**d**) $LiBr/H_2O+CaCl_2$ $LiNO_3$ at 80 °C.

As it can be seen in micrographs in Figures 7–9, the main involved of corrosion in all cases was pitting corrosion; therefore, we must take this into account when using equivalent electric circuits for EIS data fitting. Figure 10 shows the equivalent electric used to fit the EIS data of the tested steels. In this figure, R_s represents the electrolyte or solution resistance, R_{pit} is the resistance inside the pit, CPE_{pit} is the constant phase element which replaces the ideal capacitance of the pit [45], R_f is the resistance of the corrosion products film, CPE_f is the constant phase element which replaces its ideal capacitance, L is the inductance, and R_L is its resistance.

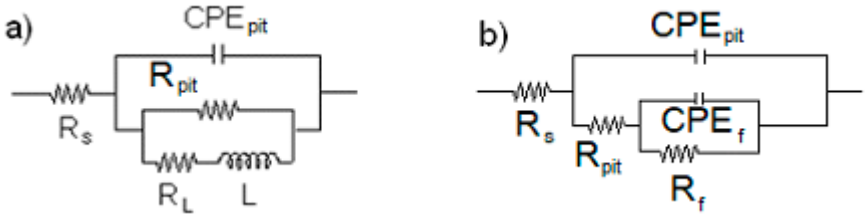


Figure 10. Electric circuits used to simulate EIS data for (**a**) 1018 carbon steel immersed in LiBr+H_2O and (**b**) 1018 carbon, 304, and 316L stainless steels in all testing conditions, except for 1018 carbon steel, immersed in LiBr+H_2O.

The obtained parameters after fitting EIS data by using the electric circuits shown in Figure 10 are given in Table 3.

From this table, it can be seen that for 1018 carbon steel, the corrosion products film resistance values, R_f, were smaller than those for the resistance inside the pit, R_{pit}, unlike what observed for type 304 and 316L stainless steels, for which the R_f values were much higher than those for R_{pit}. Conversely, the CPE_f values were lower than those of CPE_{pit}. Additionally, the R_{ct} and R_f values for 1018 carbon steel were the smallest, whereas the corresponding values for CPE_f and CPE_{pit} were the highest among the three tested steels in all tested conditions. In addition to this, 316L type stainless steel exhibited the highest R_f and R_{pit} and the lowest CPE_f and CPE_{pit} values. This was due to the type of corrosion products formed on each steel. For carbon steel, the polarization curves showed the absence of a passive layer in the LiBr/H_2O mixture, whereas a passive film was developed with the addition of $CaCl_2$ and/or $LiNO_3$. However, the passive current density did not remain constant with the applied potential, as indicated in Figure 3 for the curves obtained with the addition of $CaCl_2$ or $CaCl_2$+$LiNO_3$, whereas the passive zone was around 100 mV for data obtained with the addition of $LiNO_3$. On the other hand, the passive current density values obtained for both 304 and 316L stainless steels remained very constant with the applied potential, and the passive zones were 250 mV wide for the former and 700 mV wide for the latter.

Table 3. Electrochemical parameters from EIS data fitting.

Solution	Steel	R_{pit} (ohm cm^2)	CPE_{pit} (ohm^{-1} s^n)	n_{ct}	CPE_f (ohm^{-1} s^n)	R_f (ohm cm^2)	n_f	R_L (ohm cm^2)
LiBr+H_2O	1018	50	2.0×10^{-3}	0.6	-	-	-	39
	304	114	7.62×10^{-4}	0.9	7.51×10^{-5}	1.89×10^3	0.6	-
	316L	277	2.20×10^{-4}	0.9	3.55×10^{-5}	4.36×10^4	0.6	-
LiBr+H_2O +$CaCl_2$	1018	205	1.6×10^{-3}	0.4	1.02×10^{-3}	190	0.8	-
	304	263	7.46×10^{-4}	0.8	1.86×10^{-5}	7.12×10^3	0.5	-
	316L	297	1.19×10^{-4}	0.9	3.06×10^{-6}	1.28×10^4	0.4	-
LiBr+H_2O +$LiNO_3$	1018	165	6.23×10^{-3}	0.9	4.4×10^{-3}	102	0.9	-
	304	174	2.73×10^{-4}	0.9	6.35×10^{-5}	7563×10^3	0.4	-
	316L	323	1.5×10^{-4}	0.9	3.40×10^{-6}	1.94×10^4	0.3	-
LiBr+H_2O +$CaCl_2$ +$LiNO_3$	1018	140	6.28×10^{-3}	0.6	1.3×10^{-3}	75	0.7	-
	304	193	6.90×10^{-4}	0.9	3.35×10^{-4}	5.78×10^3	0.5	-
	316L	352	1.21×10^{-4}	0.9	6.92×10^{-5}	1.75×10^4	0.5	-

4. Conclusions

A study of the effect of $CaCl_2$ and/or $LiNO_3$ on the corrosion behavior of 1018 carbon steel and type 304 and 316L stainless steels in LiBr/H_2O at 80 °C was carried out. For the

three steels, the I_{corr} value decreased at least one order of magnitude with the addition of $CaCl_2$ and/or $LiNO_3$ to $LiBr/H_2O$. The lowest I_{corr} value for 1018 carbon steel was obtained with the addition of $CaCl_2$, whereas for both stainless steels, the lowest value was obtained with the addition of $CaCl_2$+$LiNO_3$. Carbon steel did not develop a passive film in $LiBr/H_2O$, which was induced with the addition of $CaCl_2$ and/or $LiNO_3$; both types of stainless steels formed a passive film in $LiBr/H_2O$, with or without the addition of $CaCl_2$ and/or $LiNO_3$, but the passive current density was decreased in the presence of these salts. The lowest passive current density value as well the widest passive zone was obtained for 316L type stainless steel, whereas 1018 carbon steel displayed the lowest passive current density value and the narrowest passive zone. The corrosion mechanism was controlled by the adsorption/desorption of some intermediate species for 1018 carbon steel in $LiBr/H_2O$, whereas with the addition of $CaCl_2$ and/or $LiNO_3$, it changed to a pitting corrosion process. The corrosion mechanism was charge transfer control for 304 and 316L stainless steels in $LiBr/H_2O$ and remained unaltered by the addition of $CaCl_2$ and/or $LiNO_3$. All tested materials developed a pitting type of corrosion in $LiBr/H_2O$, whereas with the addition of $CaCl_2$ and/or $LiNO_3$, the size and number of pits was modified in different ways for each material.

Author Contributions: A.K.L.-G. and J.P.-C., resources and conceptualization; J.U.-C., formal analysis and writing—review; R.L.-S. and E.S.-B., data curation and supervision; I.R., software and writing—original draft preparation; E.S.-B., validation; J.G.G.-R. and A.K.L.-G., project administration and resources; J.G.G.-R., funding acquisition. All authors have read and agreed to the published version of the manuscript.

Funding: This research received no external funding.

Data Availability Statement: All data are available upon request by contacting the corresponding author at ggonzalez@uaem.mx.

Conflicts of Interest: The authors declare that they have no conflict of interest.

References

1. Ochoa, A.A.V.; Dutra, J.C.C.; Henríquez, J.R.G.; Rohatgi, J. Energetic and exergetic study of a 10RT absorption chiller integrated into a microgeneration system. *Energy Convers. Manag.* **2014**, *88*, 545–553. [CrossRef]
2. Cézar, K.L.; Caldas, A.G.A.; Caldas, A.M.A.; Cordeiro, M.C.L.; Dos Santos, C.A.C.; Ochoa, A.A.V.; Michima, P.S.A. Development of a novel flow control system with arduino microcontroller embedded in double effect absorption chillers using the $LiBr/H_2O$ pair. *Int. J. Refrig.* **2020**, *111*, 124–135. [CrossRef]
3. Du, S.; Wang, R.Z.; Chen, X. Development and experimental study of an ammonia water absorption refrigeration prototype driven by diesel engine exhaust heat. *Energy* **2017**, *130*, 420–432. [CrossRef]
4. Mosa, M. Effect of Variable Thermo-Physical Properties of LiBr-H_2O Solution on the Performance Parameters of Horizontal Tube Absorber. *Int. J. Air-Cond. Refrig.* **2019**, *27*, 1950026. [CrossRef]
5. Cezar, K.; MacArio, A.; Cabral Dos Santos, C.A.; Ochoa, A.; Charamba Dutra, J.C. Flow Control for Absorption Chillers Using the Par H_2O/LiBr Driven in Recirculation Pumps of Low Power. *IEEE Lat. Am. Trans.* **2016**, *14*, 1624–1629.
6. Butt, I.B.; Tan, J.; Waqas, A.; Ali, M.; Javed, A.; Ali, A.Y. Effect of modified flow schemes of heat transfer fluid on the performance of a solar absorption-cooling system for an educational building in Pakistan. *Appl. Sci.* **2020**, *10*, 3327. [CrossRef]
7. Liang, C.; Hu, X. Inhibition Performance of Enhanced-Mo Inhibitor for Carbon Steel in 55% LiBr Solution. *J. Iron Steel Res. Int.* **2008**, *15*, 49–54. [CrossRef]
8. Hu, X.; Liang, C.; Huang, N. Anticorrosion Performance of Carbon Steel in 55% LiBr Solution Containing PMA/$SbBr_3$ Inhibitor. *J. Iron Steel Res. Int.* **2006**, *13*, 56–60. [CrossRef]
9. Zolfaghari, S.; Baboukani, A.R.; Ashrafi, A.; Saatchi, A. Investigation the effects of Na_2MoO_4 as an inhibitor on electrochemical corrosion behavior of 316L stainless steel in LiBr solution. *Zast. Mater.* **2018**, *59*, 108–116. [CrossRef]
10. Youssef, G.I.; El Meleigy, A.E.; Khorshed, L.A.; Attia, A.; Ashour, E.A. Inhibitive effect of benzotriazole on the corrosion and corrosion fatigue of α-Al bronze alloy in LiBr solution. *Mater. Corros.* **2018**, *69*, 1827–1836. [CrossRef]
11. El Hamid, S.E.A.; Abeer El Meleigy, E.; Attia, A.; El Fattah El Warraky, A.A.; Abd-El-Wahab, S.M. Corrosion Behaviour of Copper–nickel Alloys in LiBr Solutions: A Comparative Study. *Egypt. J. Chem.* **2020**, *63*, 907–919.
12. Yoo, J.; Han, S.; Nam, Y.; Jeong, S. Effect of shot-peening on the passive film formation and corrosion of carbon steel in LiBr aqueous solution. *J. Mech. Sci. Technol.* **2020**, *34*, 4037–4041. [CrossRef]
13. Cho, Y.; Han, S.; Seo, H.; Woo, S. Corrosion and inhibition process of carbon steel in LiBr-H_2O solution. *J. Mech. Sci. Technol.* **2019**, *33*, 2995–3000. [CrossRef]

14. Guiñon, J.L.; Garcia-Anton, J.; Pérez-Herranz, V.; Lacoste, G. Corrosion of Carbon Steels, Stainless Steels, and Titanium in Aqueous Lithium Bromide Solution. *Corrosion* **1994**, *50*, 240–246. [CrossRef]
15. Guiñón-Pina, V.; Igual-Muñoz, A.; García-Antón, J. Influence of Temperature on the Corrosion Behaviour and on the Hydrogen Evolution Reaction on Nickel and Stainless Steels in LiBr Solutions. *Int. J. Electrochem. Sci.* **2011**, *6*, 6123–6140.
16. Li, N.; Luo, C.; Su, Q. A working pair of $CaCl_2$–LiBr–$LiNO_3$/H_2O and its application in a single-stage solar-driven absorption refrigeration cycle. *Int. J. Refrig.* **2018**, *86*, 1–13. [CrossRef]
17. Li, Y.; Li, N.; Luo, C.; Su, Q. Study on a Quaternary Working Pair of $CaCl_2$-$LiNO_3$-KNO_3/H_2O for an Absorption Refrigeration Cycle. *Entropy* **2019**, *21*, 546. [CrossRef]
18. Torres-Díaz, T.; Siqueiros, J.; Coronas, A.; Salavera, D.; Huicochea, A.; Juárez-Romero, D. Performance of Li salts (LiBr + LiI + $LiNO_3$+ LiCl) for an absorption cycle of an experimental absorption heat transformer for water purification. *Desalin. Water Treat.* **2017**, *82*, 292–299. [CrossRef]
19. Yang, Y.; Lin, C.; Zhao, X.; Zhang, Y. Initial Stage Cavitation-corrosion of TA2 in Aqueous LiBr Solution. *J. Chin. Soc. Corros. Prot.* **2017**, *37*, 540–546.
20. Soliz, A.; Mayrhofer, K.J.J.; Cáceres, L. Influence of Hydrodynamic Flow Patterns on the Corrosion Behavior of Carbon Steel in a Neutral LiBr Solution. *Int. J. Electrochem. Sci.* **2018**, *13*, 10050–10075.
21. Kappes, M.A. Localized corrosion and stress corrosion cracking of stainless steels in halides other than chlorides solutions: A review. *Corros. Rev.* **2020**, *38*, 1–24. [CrossRef]
22. Irie, T.; Morihashi, D.; Hirohata, Y.; Haruna, T. Polarization Curves of Carbon Steel in Concentrated LiBr Solutions Containing LiOH and Li_2MoO_4 at Different Temperatures after Short Immersion. *Mater. Trans.* **2021**, *62*, 420–426. [CrossRef]
23. Hu, S.; Liu, R.; Liu, L.; Cui, Y.; Wang, F. Influence of temperature and hydrostatic pressure on the galvanic corrosion between 90/10 CueNi and AISI 316L stainless steel. *J. Mater. Res. Technol.* **2021**, *13*, 1402–1405. [CrossRef]
24. Muñoz-Portero, M.J.; Nachiondo, T.; Blasco-Tamarit, E.; Vicent-Blesa, A.; García-Antón, J. Potential-pH diagrams for Iron in Concentrated LiBr Solutions at 25 °C. *Corrosion* **2018**, *74*, 1102–1116. [CrossRef]
25. Fernández-Domene, R.M.; Blasco-Tamarit, E.; García-García, D.M.; Antón, J.G. Passivity Breakdown of Titanium in LiBr Solutions. *J. Electrochem. Soc.* **2014**, *161*, C25–C31. [CrossRef]
26. Guiñón-Pina, V.; Igual-Muñoz, A.; García-Antón, J. Influence of temperature and applied potential on the electrochemical behaviour of nickel in LiBr solutions by means of electrochemical impedance spectroscopy. *Corros. Sci.* **2009**, *51*, 2406–2413. [CrossRef]
27. Jiangzhou, S.; Wang, R.Z. A compressor-assisted triple-ffect H_2O-LiBr absorption cooling cycle coupled with a Rankine Cycle driven by high-temperature waste heat. *Appl. Therm. Eng.* **2001**, *21*, 1161–1168. [CrossRef]
28. Blasco-Tamarit, E.; García, D.M.; García-Antón, J. Thermogalvanic effects on the corrosion of copper in heavy brine LiBr solutions. *Corros. Sci.* **2012**, *63*, 304–311.
29. Muñoz-Portero, M.J.; García-Antón, J.; Guiñón, J.L.; Perez-Herranz, V. Corrosion of Copper in Aqueous Lithium Bromide Concentrated Solutions by Immersion Testing. *Corrosion* **2006**, *62*, 1018–1025. [CrossRef]
30. Ren, S.J.; Charles, J.; Wang, X.C.; Nie, F.X.; Romero, C.; Neti, S.; Zheng, Y.; Hoenig, S.; Chen, C.; Cao, F.; et al. Corrosion testing of metals in contact with calcium chloride hexahydrate used for thermal energy storage. *Mater. Corros.* **2017**, *68*, 1046–1056. [CrossRef]
31. Itoh, M.; Itoh, K.; Izumiya, M.; Tanno, K. Corrosion Behavior of Carbon Steels and Low Alloy Steels in Concentrated LiBr-$CaCl_2$ Solution at Elevated Temperature. *Boshoku Gijutsu* **1989**, *38*, 645–651.
32. Li, J.; Liang, C.; Huang, N. Effect of B-Mo-W Complex Inhibitor on Corrosion of Mild Steel in 55% LiBr Solution. *J. Mater. Eng. Perform.* **2015**, *24*, 4456–4461. [CrossRef]
33. Abd El Meguid, E.A.; Abd El Rehim, S.S.; Al Kiey, S.A. Inhibitory effect of cetyltrimethyl ammonium bromide on the corrosion of 904L stainless steel in LiBr solution. *Corros. Eng. Sci. Technol.* **2016**, *51*, 429–435. [CrossRef]
34. Osta-Omar, S.M.; Micallef, C. Determination of Concentration of the Aqueous Lithium–Bromide Solution in a Vapour Absorption Refrigeration System by Measurement of Electrical Conductivity and Temperature. *Data* **2017**, *2*, 6. [CrossRef]
35. Jian, S.; Lin, F.; Shigang, Z. Experimental evaluation of a direct air-cooled lithium bromide–water absorption prototype for solar air conditioning. *Appl. Therm. Eng.* **2010**, *30*, 2680–2684. [CrossRef]
36. Rahmouni, K.; Keddam, M.; Srhiri, A.; Takenouti, H. Corrosion of copper in 3% NaCl solution polluted by sulphide ions. *Corros. Sci.* **2005**, *47*, 3249–3266. [CrossRef]
37. Luo, C.; Su, Q.; Li, N.; Li, Y. Corrosion of Copper in a Concentrated $LiNO_3$ Solution at a High Temperature. *Int. J. Electrochem. Sci.* **2017**, *12*, 1896–1914. [CrossRef]
38. Guo, J.; Liang, C. Corrosion of carbon steel in concentrated $LiNO_3$ solution at high temperature. *Corros. Eng. Sci. Technol.* **2002**, *14*, 197–204.
39. Tanno, K.; Itoh, M.; Sekiya, H.; Yashiro, H.; Kumagai, N. The corrosion inhibition of carbon steel in lithium bromide solution by hydroxide and molybdate at moderate temperaturas. *Corros. Sci.* **1993**, *34*, 1453–1461. [CrossRef]
40. Kyung-Hwan, N.; Su-Il, P. Effects of sulphate, nitrate and phosphate on pit initiation of pure aluminium in HCl-based solution. *Corros. Sci.* **2007**, *49*, 2663–2675. [CrossRef]
41. Samiento-Bustos, E.; González Rodriguez, J.G.; Uruchurtu, J.; Dominguez-Patiño, G.; Salinas-Bravo, V.M. Corrosion behavior of iron-based alloys in the LiBr+ ethylene glycol+ H_2O mixture. *Corros. Sci.* **2008**, *50*, 2296–2312. [CrossRef]

42. Abd El Meguid, E.A. Pitting corrosion behavior of type 904L stainless steel in sodium bromide solutions. *Corrosion* **1997**, *53*, 623–630. [CrossRef]
43. Kaneko, M.; Isaacs, H.S. Pitting of stainless steel in bromide, chloride and bromide/chloride solutions. *Corros. Sci.* **2000**, *42*, 67–78. [CrossRef]
44. Abd El Meguid, E.A.; Mahmoud, N.A. Inhibition of bromide-pitting corrosion of type 904L stainless steel. *Corrosion* **2003**, *59*, 104–111. [CrossRef]
45. Oltra, R.; Keddam, M. Application of EIS to Pitting Corrosion. *Electrochim. Acta* **1990**, *35*, 1619–1629. [CrossRef]